Timing analysis of infrared-driven high-order harmonic generation with above-ionization attosecond pulses

Han Chieh Lee* and Tsin Fu Jiang

Institute of Physics, National Chiao Tung University, 1001 University Road, Hsinchu 30010, Taiwan
**Corresponding author: hclee@mail.nctu.edu.tw*

Received December 17, 2012; revised March 12, 2013; accepted March 27, 2013;
posted March 28, 2013 (Doc. ID 181919); published April 23, 2013

We theoretically study infrared (IR)-driven high-order harmonic generation (HHG) assisted by attosecond pulses with a central energy above the atomic ionization threshold. We provide a clear physical picture for controlling HHG using the time delay between the attosecond pulses and the IR laser reported by Faria *et al.* [Phys. Rev. A **74**, 053416 (2006)]. This physical picture also indicates that the combined attosecond pulses and IR laser can help resolve the dynamics of ionized electrons from time-dependent harmonic spectra. We present the quantum effect on HHG as an example. While leaving parent ions, ionized electrons can still emit harmonics in the semiclassically forbidden situation. The two-color excitation provides a practical method to observe the quantum effect experimentally. Furthermore, in our work, attosecond pulses and an IR field are considered with a realistic pulse shape, which shows a quantitatively important effect in controlling harmonic spectra. Accordingly, a guide to optimize the control capability for HHG is presented, and a method to determine the IR carrier-envelope phase based on the pulse-shape effect on the HHG is also proposed.

OCIS codes: (020.2649) Strong field laser physics; (020.4180) Multiphoton processes; (190.2620) Harmonic generation and mixing; (340.7480) X-rays, soft x-rays, extreme ultraviolet (EUV).
http://dx.doi.org/10.1364/JOSAB.30.001294

1. INTRODUCTION

High-order harmonic generation (HHG) is a highly nonlinear optical process in a medium that can be used to generate extremely ultraviolet (XUV) light from an infrared (IR) laser. Generally, high harmonics in intensity decrease quickly at low orders, then form a plateau over a number of orders, and finally decay rapidly after a cutoff order. By the XUV harmonic plateau, an optical pulse with an attosecond duration can be created [1,2]. An attosecond pulse (attopulse) can be used to resolve electronic dynamics in atomic scales [3–9], such as atomic inner-shell dynamics [3], real-time tunneling observation [4], and time-resolved Fano resonance [5,6]. On the other hand, attopulses are also powerful tools for controlling electronic dynamics in atoms [10–20]. Until now, they have been applied to perform electron wave packet interferometry [10,11], attosecond control of atomic ionization [12–14], and molecular dissociation [15,16]. Interestingly, this extremely short pulse can also be used to control a new source of HHG [17–21]. This is because the basic mechanism of HHG from atoms or molecules can be described in three electronic steps, i.e., ionization, acceleration, and recombination (the three-step model) [22,23]. Thus, if one of these three steps is controlled, HHG could become a controllable source.

Schafer *et al.* [18] were the first to propose using attopulses to control the quantum path and HHG. To control HHG with attopulses, the central energy of attopulses to cross the atomic ionization threshold plays a particular role. If the central energy of the attopulses is below the ionization threshold, the attopulses excite an unperturbed atom to higher bound states. When an IR laser is injected later, the excited atom can then be easily ionized, producing a considerable amount of continuum electrons. Hence, the HHG is dramatically enhanced [20,24,25] compared with the case without below-ionization (BI) attopulses. However, the HHG including the cutoff energy and plateau height is not sensitive to the time delay between the attopulses and the IR field, which is simply called the IR delay phase later [26]. Conversely, if the central energy of the attopulses is above the ionization threshold, the HHG becomes sensitive to the IR delay phase. Faria *et al.* [17] showed that a wide variation of cutoff energy from $I_p + 1.8U_p$ to $I_p + 2.5U_p$ can be achieved together with a large change in plateau height as the IR delay phase changes, where I_p is the ionization potential and U_p is the ponderomotive energy at the IR frequency. This result was explained by the interference effect between various quantum orbits of electrons [17], which can show a coincident cutoff energy as the IR delay phase varies. However, this interpretation leaves some questions unanswered. For example, why is the cutoff energy lower than $I_p + 3.17U_p$ predicted by the three-step model? Does this type of HHG satisfy the three-step model? Why is the controlled HHG sensitive to the IR delay phase? These questions arise because the result shows behaviors that significantly differ from another kind of controlling the HHG by two-color (800 nm + 1300 nm) IR fields [27]. In the later case, the cutoff energy becomes higher than $I_p + 3.17U_p$, and can be written in a formula that fits the three-step model with only a modification for the two-color IR fields. This indicates that the cutoff energy [27] is sensitive to the intensity ratio between the two-color IR fields rather than their IR delay phase. However, if the second color 1300 nm is replaced with 400 nm, the cutoff energy caused by the two-color excitation (800 + 400 nm) can recover to depend on the IR delay phase again [28].

In this paper, we systematically study the IR-driven HHG with above-ionization (AI) attopulses, and provide an alternative picture of the control mechanism of HHG. In this picture, the reduced and controllable cutoff energy can be clearly elucidated based on the timing analysis of HHG [29–31], which coincides with the three-step model well. Particularly, this picture also indicates that an AI single attosecond pulse (SAP) is a good tool for resolving the IR-driven dynamics of ionized electrons from the time-dependent harmonic spectrum. This method can reveal a quantum effect on the harmonic emission that is beyond the semi-classical prediction of the three-step model. While leaving away from its parent ion, the ionized electrons can still emit harmonics even when no collision between electrons and ions occurs. The result agrees with that by Pérez-Hernández and Plaja [32], who used one driving IR field. We use the combined attopulses and IR field to provide a practical method to observe this effect. Furthermore, we consider that the attopulses and IR field have realistic pulse shapes, and study their effects on HHG. These results are compared with those by Faria *et al.* [17], who analytically considered the attopulses and IR field as a Dirac comb and a continuous wave, respectively. Our results show a good agreement with those by Faria *et al.* [17] qualitatively. However, the realistic shapes of attopulses and the IR field have a quantitatively considerable effect on the harmonic spectra. We will interpret how to optimize control capability using the attopulse's shape, and illustrate that the IR field has a particularly strong pulse-shape effect on the harmonic emission. Based on this strong effect, a possibility of finding the IR delay phase from the harmonic spectra is also proposed. The remainder of this paper is organized as follows. Section 2 describes the theoretical method. Section 3 provides results and a discussion. Finally, Section 4 offers the conclusion.

2. THEORETICAL METHOD

Unless otherwise specified, atomic units (a.u.) are used in this paper. In the controlled HHG, the ionization is dominated by the attopulses, whereas the acceleration is caused by the IR field. Thus, the atomic transition amplitude can be written as [17,33]

$$T(t) = -i\int_{-\infty}^{t} \mathrm{d}t_1 \langle \psi_{\mathbf{k}}^{\mathrm{CV}}(\mathbf{r},t_1)|V_{\mathrm{XUV}}(t_1)|\psi_g(\mathbf{r},t_1)\rangle, \tag{1}$$

where $\psi_g(\mathbf{r},t_1) = \varphi_g(\mathbf{r})\exp(-i\omega_g t_1)$, $\varphi_g(\mathbf{r})$ is the ground-state wave function and ω_g is the ground-state energy of unperturbed Hamiltonian $\hat{H}_0 = \frac{1}{2}\hat{\mathbf{p}}^2 + V_M(\mathbf{r})$, and $V_M(\mathbf{r})$ is the atomic model potential within the single-active-electron approximation (SAE) [34]. The interaction $V_{\mathrm{XUV}}(t_1) = \frac{1}{c}\mathbf{A}_{\mathrm{atto}}(t_1)\cdot\hat{\mathbf{p}}$, and $\mathbf{A}_{\mathrm{atto}}(t_1)$ is the vector potential of the AI attopulses, which is equal to $-c\int_{-\infty}^{t_1}\mathbf{E}_{\mathrm{atto}}(t')\mathrm{d}t'$,

$$\mathbf{E}_{\mathrm{atto}}(t') = \sum_{\xi}[(-1)^{\xi}\mathbf{E}_s(t'-\xi T_h)]\exp\left[-2\ln 2\left(\frac{t'}{\tau_T}\right)^2\right], \tag{2a}$$

$$\mathbf{E}_s(t') = \hat{z}E_X\sin(\omega_X t')\exp\left[-2\ln 2\left(\frac{t'}{\tau_X}\right)^2\right], \tag{2b}$$

where $T_h = \pi/\omega_{\mathrm{IR}}$, and ω_{IR} is the IR energy at 1.55 eV. Unless otherwise specified, the attopulse's width τ_X is set to 0.3 fs and the attopulse's central energy ω_X is set to 35 eV, which is approximately 10 eV higher than I_p (He). We choose helium as the target atom, and adapt the model potential from the work of Tong and Lin [34]. With the index ξ and the parameter τ_T, attopulses can be tuned from SAP to an attosecond pulse train (APT) [33]. For SAP, ξ is set as −1, and τ_T is set to infinity, whereas for APT, ξ sums over −10 to 10, and $\tau_T = 5$ fs. The attopulse's peak electric field E_X is set so that its peak intensity is 5×10^{13} W/cm^2. To improve the Volkov wave used by Faria *et al.* [17], we use the Coulomb–Volkov (CV) wave as IR-dressed continuum states, where the atomic potential is considered adiabatically. The CV wave is given by

$$\psi_{\mathbf{k}}^{\mathrm{CV}}(\mathbf{r},t_1) = \varphi_{\mathbf{k}}(\mathbf{r})\exp\left[-i\int_{-\infty}^{t_1}E_{\mathbf{k}}(t')\mathrm{d}t'\right], \tag{3}$$

where $\varphi_{\mathbf{k}}(\mathbf{r}) = \sum_{l=0}^{\infty}\sum_{m_l=-l}^{l} i^l e^{-i(\sigma_l+\delta_l)}R_{kl}(r)Y_{lm_l}(\Omega_{\mathbf{r}})Y_{lm_l}^*(\Omega_{\mathbf{k}})$, and $\mathbf{k}$ is the electron's wave vector. $R_{kl}(r) = \sqrt{(2/\pi k)}(u_l(r)/r)$. The equation for $u_l(r)$ with an asymptotic relation can be found in [33], and can be solved using the Numerov method. Here σ_l and δ_l are the Coulomb and short-range phase shifts, respectively. $E_{\mathbf{k}}(t') = [\mathbf{k} + (1/c)\mathbf{A}_{\mathrm{IR}}(t')]^2/2$.

$$\mathbf{A}_{\mathrm{IR}}(t') = \hat{z}\frac{cE_{\mathrm{IR}}}{\omega_{\mathrm{IR}}}\exp\left[-2\ln 2\left(\frac{t'}{\tau_{\mathrm{IR}}}\right)^2\right]\cos(\omega_{\mathrm{IR}}t'+\phi_d), \tag{4}$$

where the IR pulse's width τ_{IR} is 5 fs. The IR delay phase ϕ_d, also called the carrier-envelope phase, is equal to $-\omega_{\mathrm{IR}}t_d$, where t_d is the time delay between the attopulses and the IR field. The IR peak electric field E_{IR} is set so that its peak intensity is 5×10^{14} W/cm^2.

In the work of Faria *et al.* [17], they used neon as a target atom and set the intensity of attopulses at 10^{13} W/cm^2. Here we make a different choice from theirs to ensure that the ionization is dominated by attopulses in all cases we discuss. Thus, we select a helium target for its higher ionization potential ($I_p = 24.6$ eV) than that of neon ($I_p = 21.6$ eV) to reduce the IR ionization, and also raise the attopulse's intensity to 5×10^{13} W/cm^2, while the IR intensity remains the same as theirs [17]. Our choice can also be confirmed by the result of the time-dependent Schrödinger equation (TDSE) [18], where a helium target was used with an attopulse's intensity of 10^{13} W/cm^2 and IR intensity of 4×10^{14} W/cm^2. Moreover, because the attopulse's energy in the TDSE's work [18] partially covers harmonics below the ionization threshold (H11–H15), the 2p and 3p states (in the SAE approximation) can be excited, and these excited bound states also contribute to HHG after IR excitation. Thus, if the BI harmonics are neglected, the required minimum attopulse's intensity by the TDSE is further reduced ($<10^{13}$ W/cm^2). In our calculation, the average plateau height of the HHG caused by the IR is 10^{-9} (a.u.), which is calculated by Eq. (6) except with $V_{\mathrm{XUV}}(t_1)$ replaced with $V_{\mathrm{IR}}(t_1)$. This value is at least one order lower than those caused by the attopulses. Thus, to fit all our cases, the required minimum attopulse's intensity is 5×10^{12} W/cm^2.

With the transition amplitude in Eq. (1), the atomic wave function under the excitation of AI attopulses and the IR field can be constructed by

$$\Psi(\mathbf{r},t) = \psi_g(\mathbf{r},t) + \int \mathrm{d}^3\mathbf{k} T(t)\psi_{\mathbf{k}}^{\mathrm{CV}}(\mathbf{r},t). \quad (5)$$

Consequently, the dipole moment for the harmonic emission can be expressed as

$$\begin{aligned} d(t) &\equiv \langle\Psi(t)|z|\Psi(t)\rangle \\ &= -i\int_{-\infty}^{t}\mathrm{d}t_1\int \mathrm{d}^3\mathbf{k}\langle\psi_g(t)|z|\varphi_{\mathbf{k}}\rangle\langle\varphi_{\mathbf{k}}|V_{\mathrm{XUV}}(t_1)|\psi_g(t_1)\rangle \\ &\quad\times\exp\left[-i\int_{t_1}^{t}E_{\mathbf{k}}(t')\mathrm{d}t'\right] + \mathrm{c.c.}, \end{aligned} \quad (6)$$

where multiple integration is calculated accurately without using stationary phase approximation [23]. Here, c.c. denotes the complex conjugate. For brevity, the spatial variable ($\mathbf{r}$) is no longer shown in the bracket.

HHG's spectrum is then given by

$$P(\omega) = \left|\int_{-\infty}^{\infty}\mathrm{d}(t)\exp(-i\omega t)\mathrm{d}t\right|^2. \quad (7)$$

HHG's spectrum as a function of emission time can be obtained using the wavelet transform [29–31]. The detailed spectral and temporal structure of HHG's spectrum, also called the wavelet spectrum, can be calculated as

$$P_W(t,\omega) = \left|\int_{-\infty}^{\infty}\mathrm{d}(t')\sqrt{\omega}W[\omega(t'-t)]\mathrm{d}t'\right|^2, \quad (8)$$

where $W[\omega(t'-t)]$ is the mother wavelet, and the Morlet wavelet $W(x) = \tau^{-1/2}\exp(ix)\exp(-x^2/2\tau^2)$ is used with $\tau = 15$ [31].

3. RESULTS AND DISCUSSION

A. Control of Cutoff Energy

In the following, the time interval [,] is always in units of the optical cycle (*o.c.*) of the IR field, and is no longer written for brevity. Figure 1(a) schematically shows the vector potentials of the SAP and IR field for the case of $\phi_d = 0.5\pi$, where the SAP is triggered at the zero of the IR vector potential. We plot the vector potential in this diagram instead of the electric field because the final momentum p_f of the ionized electrons is closely related to the IR vector potential according to the streaking effect $p_f = p_i - A_{\mathrm{IR}}(t)/c$ with p_i being the initial momentum. This is helpful for below physical interpretation.

At $t = -0.5\,o.c.$, the SAP creates an ionized electron, which is then driven by the IR field. In the half-cycle

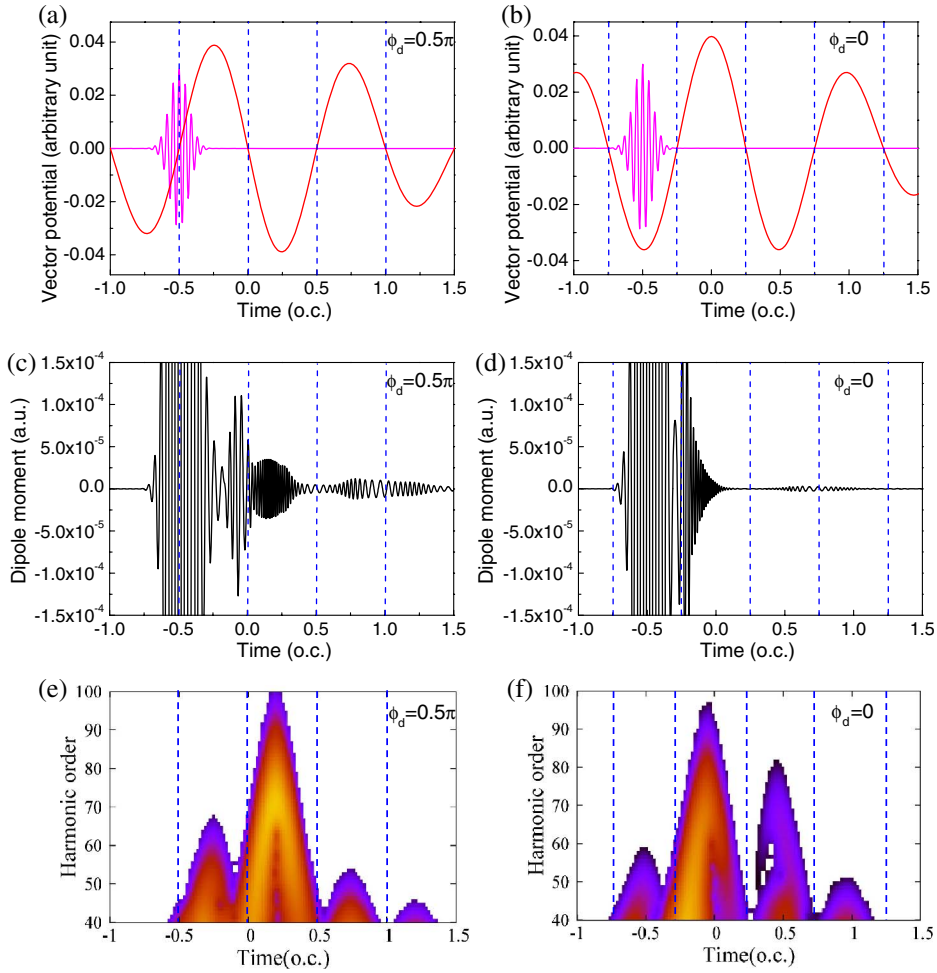

Fig. 1. Schematic diagram for the SAP and IR vector potentials for (a) $\phi_d = 0.5\pi$ and (b) $\phi_d = 0$. Timing HHG's dipole moment for (c) $\phi_d = 0.5\pi$ and (d) $\phi_d = 0$. HHG's wavelet spectrum for (e) $\phi_d = 0.5\pi$ and (f) $\phi_d = 0$. The horizontal axis denotes the emission time in units of the IR *o.c.* The peak intensities of the SAP and the IR field are 5×10^{13} W/cm^2 and 5×10^{14} W/cm^2, respectively, where $\tau_X = 0.3$ fs, $\omega_X = 35$ eV, and $\omega_{IR} = 1.55$ eV.

[−0.5, 0], the IR vector potential is always positive, thus driving the electron away from its parent ion. The IR vector potential becomes negative as time crosses the point of $t = 0$, and the electron is driven reversely and returns to collide with its parent ion. Hence, a strongly chirped dipole moment occurs in the next half-cycle [0, 0.5], as Fig. 1(c) shows. Specifically, high-order harmonics are generated, and Fig. 1(e) shows the detailed temporal and spectral diagram. We can see that the cutoff harmonic order increases as time departs from $t = 0$ and reaches a maximum at $t = 0.25\,o.c.$, which corresponds to the peak of the IR vector potential. The cutoff harmonic order then decreases until $t = 0.5\,o.c.$, corresponding to a zero IR vector potential exactly. The close match between the cutoff harmonic order and the IR vector potential indicates that the IR vector potential is indeed a good quantity to analyze the time-dependent harmonic spectrum. The reverse is also true, and perhaps more important in applications. In other words, under the SAP + IR excitation, the time-dependent harmonic spectrum can be used to identify the IR vector potential because of their timing match. With the time-dependent IR vector potential, the dynamics of ionized electrons can be acquired through the streaking effect. Accordingly, we can deduce that the ionized electron for $\phi_d = 0.5\pi$ takes an average of 0.75 *o.c.* to perform acceleration because the ionized electron is born at $t = -0.5\,o.c.$ and becomes fastest at $t = 0.25\,o.c.$

The acceleration time of ionized electrons varies as the IR delay phase changes. For $\phi_d = 0$, the SAP remains at $t = -0.5\,o.c.$, but becomes triggered at the peak of the IR vector potential, as Fig. 1(b) shows. After the SAP, an ionized electron is created and driven by the IR field; however, only 0.25 *o.c.* later does the IR vector potential change direction, and this is in contrast with $\phi_d = 0.5\pi$ (with 0.5 *o.c.*). The ionized electron then makes a strongly chirped dipole moment in the interval [−0.25, 0.25], as Fig. 1(d) shows, and the emission of the maximum cutoff harmonics occurs at $t = 0$, as Fig. 1(f) shows. In other words, the ionized electron takes only an average of 0.5 *o.c.* to accelerate, which is 0.25 *o.c.* shorter than $\phi_d = 0.5\pi$. Hence, a shorter electronic acceleration time produces a lower cutoff energy for $\phi_d = 0$ than for $\phi_d = 0.5\pi$, which is in agreement with the prediction by Faria *et al.* [17].

Before the following topics, note that our work uses the CV wave to improve the Volkov wave, but the CV wave is still an approximation that adiabatically includes the Coulomb interaction in the IR-dressed continuum state. In fact, no exact analytic solution for the IR-dressed continuum state exists. This adiabatic approximation fails to consider the Coulomb-laser (CL) coupling effect, thus making corresponding results still qualitative. To improve the adiabatic approximation, the Eikonal–Volkov (EV) wave [35–37] can be considered when the Coulomb interaction is not strong. The EV wave is derived within the Eikonal approximation, which is closely related to the Wentzel–Kramers–Brillouin (WKB) method. By expanding the wave function into different orders of $\hbar$, the Coulomb interaction can be treated perturbatively, and then its correction is taken into the phase part of IR-dressed continuum states to include the CL coupling effect, which currently shows a particular role in the accuracy of the attosecond streak camera for time-resolved photoionization measurement [38,39].

B. Quantum Effect on HHG

In the previous results, we also find an unusual harmonic emission in the wavelet spectra. Based on the three-step model, the ionized electron born at a zero IR vector potential requires at least 0.5 *o.c.* to emit harmonics because of the round-trip process. However, Fig. 1(e) shows that harmonic emission can still occur in the semi-classically forbidden interval [−0.5, 0], where the electron runs away from its parent ion. Similarly, the ionized electron born at the peak of the IR vector potential requires at least 0.25 *o.c.* semi-classically, but Fig. 1(f) also shows harmonic emissions in the interval [−0.5, −0.25]. The unusual emission is due to the quantum effect on HHG. Because of the wave behavior of electrons, the spreading electronic wave packet can overlap its parent ion at any time. Thus, even if the electron leaves its parent ion, a nonzero overlapping integral between the continuum and the ground states [Eq. (6)] still makes recombination possible. This result is in agreement with those by Pérez-Hernández and Plaja [32]. The XUV + IR excitation can successfully be used to explore the quantum effect because of the extremely short width of SAP, which makes the ionization process accomplished within a very small fraction of the IR cycle. Thus, subsequent IR-driven acceleration of ionized electrons can take place without the ionization process. This is unlike the one-color excitation [32], which mixes the acceleration with the ionization process. The advantage here is that the wavelet spectrum is only determined by IR-driven acceleration. Hence, the recombination of ionized electrons with their parent ions in the semi-classically forbidden situation can be time resolved by the wavelet spectrum theoretically or by the time-dependent harmonic spectrum experimentally.

C. Attopulse Shape Effect on HHG

To study the control mechanism of HHG in detail, Fig. 2(b) shows the SAP + IR harmonic spectra with the same conditions as those in Fig. 1. The red-solid and black-dashed lines in this figure denote the results of $\phi_d = 0.5\pi$ and $\phi_d = 0$, respectively. The spectrum of $\phi_d = 0.5\pi$ has a broader cutoff energy than the spectrum of $\phi_d = 0$, but with a lower plateau height. This dependence is in good qualitative agreement with the results by Faria *et al.* [17]. However, on a quantitative side, a relatively significant difference exists between our results and theirs. For example, our cutoff energy shows a weak variation from $I_p + 2.60U_p$ to $I_p + 2.86U_p$ as the IR delay phase changes. This is unlike the strong variation from $I_p + 1.8U_p$ to $I_p + 2.5U_p$ in their results [17]. In addition, our cutoff energy for each IR delay phase is larger than their corresponding cutoff energy. Both discrepancies are due to the realistic shape effect of attopulses, which was neglected in their work [17]. To illustrate this effect, Fig. 2(a) shows the harmonic spectra with the SAP's width at a current experimental limit of 80 as [40], where the cutoff energy of $\phi_d = 0$ greatly shrinks to $I_p + 2.24U_p$, whereas that of $\phi_d = 0.5\pi$ remains unchanged. In other words, the cutoff energy recovers to strongly depend on the IR delay phase. In contrast, if we enlarge the SAP's width to 600 as, the cutoff energy of $\phi_d = 0$, as shown in Fig. 2(c), approaches to that of $\phi_d = 0.5\pi$, which is unable to control the cutoff energy.

The effect of the SAP's width can be explained using Fig. 1(b). Ideally, if the SAP has a Dirac-delta shape, the ionized electron born at $t = -0.5\,o.c.$ has exactly 0.5 *o.c.* to

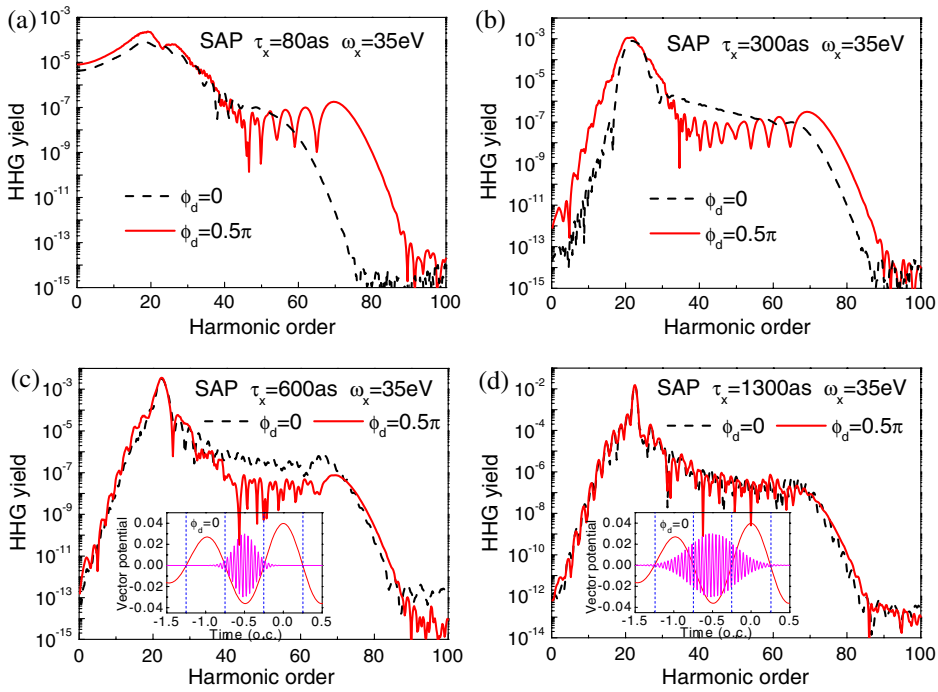

Fig. 2. Attopulse shape effect on the SAP + IR harmonic spectra at distinct attopulse widths (a) $\tau_X = 80$ as, (b) $\tau_X = 300$ as, (c) $\tau_X = 600$ as, and (d) $\tau_X = 1300$ as, where $\omega_X = 35$ eV. Red-solid and black-dashed lines denote the results of $\phi_d = 0.5\pi$ and $\phi_d = 0$, respectively. Insets of (c) and (d) show the schematic diagram for the SAP and IR vector potentials at $\tau_X = 600$ as and $\tau_X = 1300$ as, respectively, where the horizontal axis is in units of the IR *o.c.*

accelerate before arriving at the fastest velocity at $t = 0$, as discussed before. However, because the SAP has a finite width, some ionized electrons are born before $t = -0.5\,o.c.$, and thus they have a longer acceleration time than ionized electrons born at exactly $t = -0.5\,o.c.$, which then makes the cutoff energy increase. If the SAP's width increases to 600 as, the SAP shown in the inset of Fig. 2(c) even spreads over $t = -0.75\,o.c.$; in other words, the ionized electron can have 0.75 *o.c.* to accelerate, and thus its cutoff energy approaches that of $\phi_d = 0.5\pi$. If the SAP's width is further enlarged to 1300 as, both the cutoff energy and the plateau height become almost indistinguishable between the two IR delay phases, as Fig. 2(d) shows. Otherwise, the cutoff energy for $\phi_d = 0.5\pi$ is insensitive to the SAP's width because the ionized electron born at $t = -0.5\,o.c.$ already has a maximum acceleration time (0.75 *o.c.*). If ionized electrons are born earlier than $t = -0.5\,o.c.$ because of a finite SAP's width [Fig. 1(a)], they run away from their parent ion until $t = -0.5\,o.c.$ and return to emit maximum cutoff harmonics at $t = -0.25\,o.c.$ Thus, their acceleration times are shorter than those born at exactly $t = -0.5\,o.c.$ Conversely, if ionized electrons are born later than $t = -0.5\,o.c.$, they emit maximum cutoff harmonics at $t = -0.25\,o.c.$ and also have a shorter acceleration time than those born at exactly $t = -0.5\,o.c.$ Consequently, the cutoff energy for $\phi_d = 0.5\pi$ remains unchanged when the SAP has a finite width.

D. Control of Plateau Height

This section presents an analysis of plateau height control. The plateau height generally can exhibit a nearly one-order variation as the IR phase changes [Figs. 2(b) and 2(c)], except for an extremely short SAP's width [Fig. 2(a)]. Interestingly, the variation of the plateau height can be enhanced by increasing the central energy of the SAP. Figure 3(b) shows the harmonic spectrum with the same conditions as those in Fig. 2(b) except that ω_X increases to 50 eV. The variation of the plateau height is clearly enhanced compared with that in Fig. 2(b). This enhancement can also apply to the extremely short SAP's width shown in Fig. 3(a), with ω_X at 50 eV. The enhancement can be interpreted as follows. As the central energy of the SAP increases, the transition amplitude $\langle\varphi_k|V_{\mathrm{XUV}}(t_1)|\psi_g(t_1)\rangle$ in Eq. (6) decreases, and thus lowers the plateau height, which is valid for all IR delay phases. However, for $\phi_d = 0$, the decreased transition amplitude can be compensated for by the IR streaking effect. The streaking effect is strong at the given IR phase because of the ionized electron born at peaks of the IR vector potential. This effect gives the ionized electron an initial momentum from the IR field to move toward a higher energy distribution, and therefore raises the plateau height after recombination. As a result, the variation of the plateau height between the two IR phases is enhanced as the central energy of the SAP increases. This idea is also supported by the streaking effect, making the plateau height at $\phi_d = 0$ smoother than that at $\phi_d = 0.5\pi$, which is particularly evident in Fig. 2(b) and Figs. 4(c) and 4(d).

In the previous work [17], Faria *et al.* considered an atom to be excited by the APT. To see the APT's effect, Figs. 3(c) and 3(d) show the APT + IR harmonic spectra, in which the other conditions are the same as those in Figs. 3(a) and 3(b), respectively. With the APT, the harmonic order becomes selective in the spectrum (i.e., the odd order enhances, whereas the even order weakens in general). This is because of the interference effect among ionized electrons born by distinct bursts of the APT, leading to a multipeak structure. However, this interference effect does not change the magnitude of the cutoff energy and the dependence of the plateau height on the

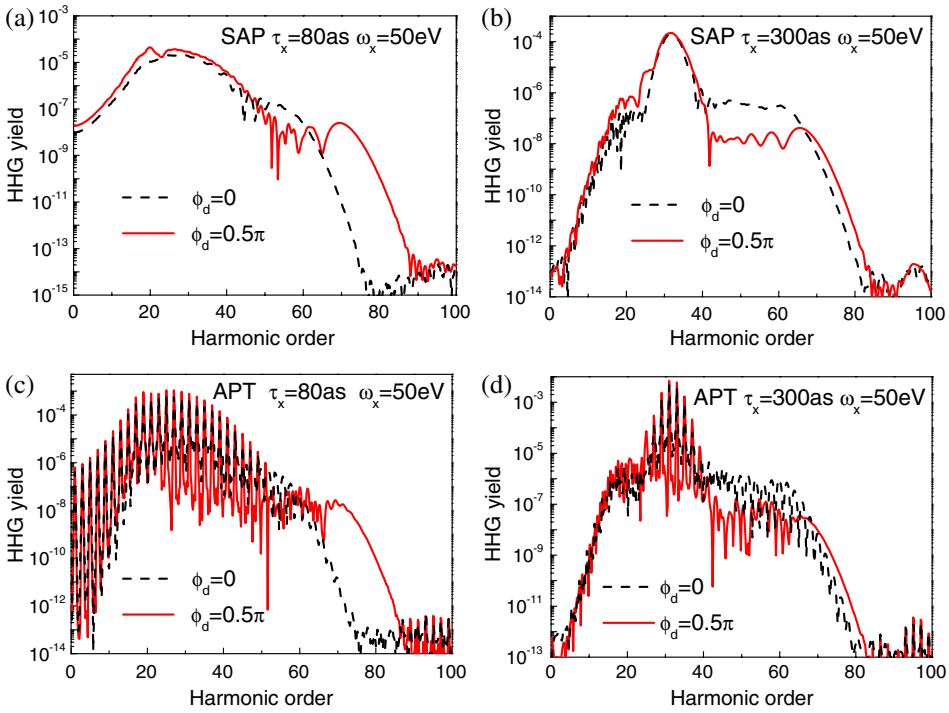

Fig. 3. SAP + IR harmonic spectra for (a) $\tau_X = 80$ as and (b) $\tau_X = 300$ as, where $\omega_X = 50$ eV. APT + IR harmonic spectra for (c) $\tau_X = 80$ as and (d) $\tau_X = 300$ as, where $\omega_X = 50$ eV and $\tau_T = 5$ fs. Red-solid and black-dashed lines denote the results of $\phi_d = 0.5\pi$ and $\phi_d = 0$, respectively.

IR delay phase. The spectrum of $\phi_d = 0.5\pi$ still has a broader cutoff energy but a lower plateau height than that of $\phi_d = 0$. Thus, the control mechanism of the HHG discussed earlier also holds for the APT's case.

E. IR Pulse-Shape Effect on HHG

Unlike the attopulse shape, the IR pulse shape has a positive effect on the control of the cutoff energy. The IR shape effect is considered by changing the SAP's trigger time, whereas the IR field remains unchanged, as shown in Fig. 4(a). The red-solid, green-dashed, and blue-dash-dotted lines in this figure denote the SAP triggered at $t = -0.5\,o.c.$ ($\xi = -1$), $0\,(\xi = 0)$, and 0.5 $o.c.$ ($\xi = 1$), respectively, and $\tau_X = 300$ as and $\phi_d = 0.5\pi$. Because they are born at different times, the ionized electrons experience distinct sections of the IR pulse, consequently enabling an examination of the IR pulse-shape effect. Figure 4(c) shows the corresponding harmonic spectra. The cutoff energy varies significantly when the SAP's trigger time changes. The dramatic effect can have a clear interpretation. Based on a previous discussion [Figs. 1(a) and 1(e)], the ionized electrons born at a zero IR vector potential require 0.75 $o.c.$ to emit maximum cutoff harmonics. Thus, the maximum cutoff energy for each SAP's trigger time t_i is related to $|\mathbf{A}_{\mathrm{IR}}(t_i + 0.75)|^2$, where t_i is in $o.c.$ units. Namely, the cutoff energies for the SAP triggered at $t_i = -0.5\,o.c.$, 0, and 0.5 $o.c.$ are determined by $|\mathbf{A}_{\mathrm{IR}}(0.25)|^2$, $|\mathbf{A}_{\mathrm{IR}}(0.75)|^2$, and $|\mathbf{A}_{\mathrm{IR}}(1.25)|^2$, respectively. Because of its Gaussian shape, $\mathbf{A}_{\mathrm{IR}}(t)$ rapidly decays for $t > 0$, and has a considerable effect on the cutoff energy. Similarly, ionized electrons born at peaks of the IR vector potential ($\phi_d = 0$), as shown in Fig. 4(b), require 0.5 $o.c.$ to emit maximum cutoff harmonics. Thus, the maximum cutoff energy is related to $|\mathbf{A}_{\mathrm{IR}}(t_i + 0.5)|^2$. The corresponding harmonic spectra shown in Fig. 4(d) also illustrate a dramatic change in the cutoff energy. Thus, the IR shape effect is really an efficient way to control the cutoff energy.

F. IR Carrier-Envelope Phase from HHG

The strong IR pulse-shape effect can also have a reverse application. With the harmonic spectrum, the IR pulse's information, including its phase, can be acquired from the dramatic change in the cutoff energy with the SAP's trigger time. Particularly, measuring the IR delay phase (i.e., carrier-envelope phase) is an important issue for frequency combs consisting of discrete and equally spaced components with absolute frequencies [41,42], which constitute a basis for high-precision metrology and receive considerable attention [43,44]. The IR phase is generally not constant from pulse to pulse because the group and phase velocities differ inside the laser cavity. The IR phase is locked unless a feedback electronic module is equipped [41,42], which requires the IR phase as a consecutive input. The IR phase is often measured using the so-called f-to-2f heterodyne technique [41,42]. This measurement can also be performed by anisotropic photoelectron spectra excited by either a linearly [45] or a circularly [46] polarized few-cycle IR field. With the help of attopulses, direct measurement of the IR field using the streaking effect is also possible [47], which consequently enables us to acquire the IR phase. However, to date, measuring the IR phase from the harmonic spectrum has not been proposed.

To interpret this idea, Fig. 5(a) shows the harmonic spectra as a function of the SAP's trigger time, where $\tau_X = 80$ as and $\phi_d = 0.5\pi$. First, the harmonic spectra vary clearly with the SAP's trigger time, and the harmonic peaks and valleys are distinguishable. Next, harmonic peaks occur at approximately $0.5n\,o.c.$ with n being an integer, whereas harmonic valleys appear at approximately $(0.5n + 0.25)\,o.c.$ Suppose an experiment shows a result like this; one can deduce that the zero IR

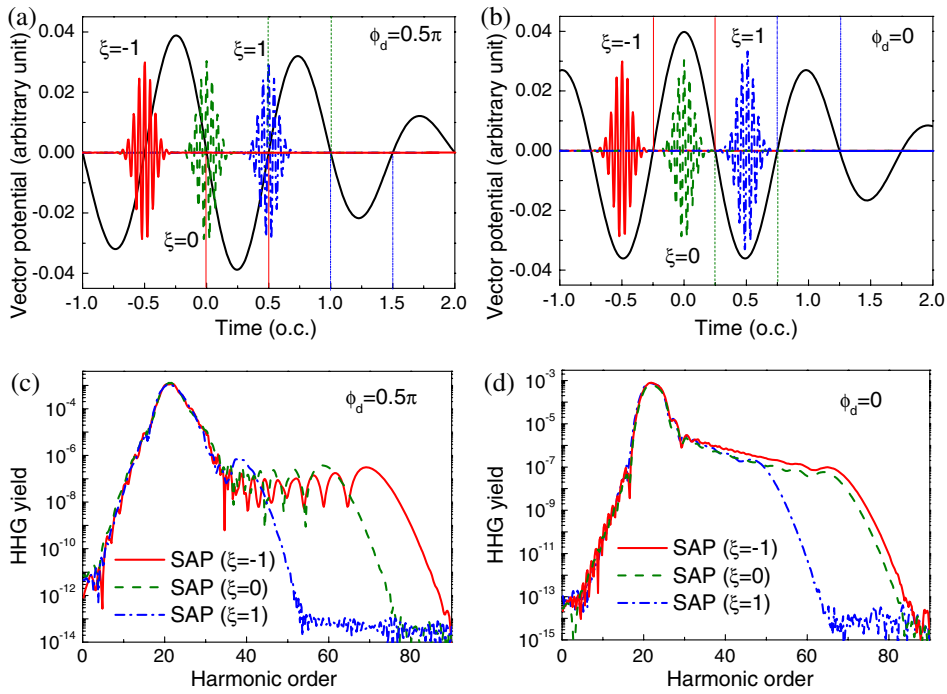

Fig. 4. IR pulse-shape effect on the harmonic spectra. Schematic diagram for the SAP and IR vector potentials with distinct SAP trigger times for (a) $\phi_d = 0.5\pi$ and (b) $\phi_d = 0$, where the horizontal axis is in units of the IR *o.c.* SAP + IR harmonic spectra with distinct SAP's trigger times for (c) $\phi_d = 0.5\pi$ and (d) $\phi_d = 0$. Red-solid, green-dashed, and blue-dash-dotted lines denote the SAP triggered at $t = -0.5\,o.c.$ ($\xi = -1$), $t = 0$ ($\xi = 0$), and $t = 0.5\,o.c.$ ($\xi = 1$), respectively. $\tau_X = 0.3$ fs and $\omega_X = 35$ eV.

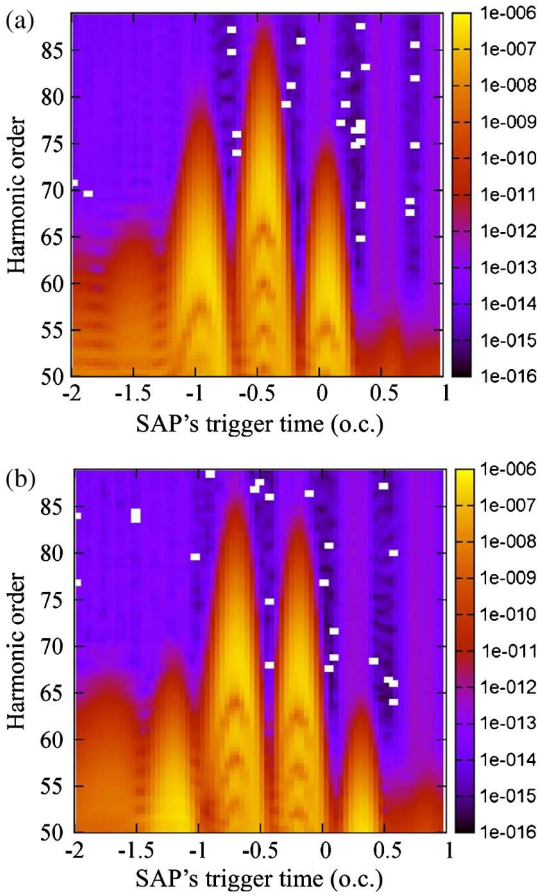

Fig. 5. SAP + IR harmonic spectra as a function of the SAP's trigger time for (a) $\phi_d = 0.5\pi$ and (b) $\phi_d = 0$, where $\tau_X = 80$ as, $\omega_X = 35$ eV, and the horizontal axis is in units of the IR *o.c.*

vector potential is at $0.5n\,o.c.$ because the ionized electrons born here result in harmonic peaks. Thus, the IR phase should be $\pm 0.5\pi$ with a cosine carrier wave. The choice of the $\pm$sign of the IR phase can be determined by comparing calculated results to judge between the two cases. In contrast, if the IR phase becomes zero, as shown in Fig. 5(b), harmonic peaks occur at approximately $(0.5n + 0.25)\,o.c.$, whereas harmonic valleys appear at approximately $0.5n\,o.c.$ Suppose an experiment shows a result like this; one can deduce that the peaks of the IR vector potential are at $0.5n\,o.c.$ because the ionized electrons born here result in harmonic valleys. Thus, the IR phase should be zero or π with a cosine carrier wave. Similarly, the two choices can be determined with the help of calculations. For the IR phase between 0 and 0.5π, the method is still applicable by using the trigger time of harmonic peaks or valleys to deduce the profile of the IR vector potential. In a series of calculations, the estimated accuracy of the IR phase is approximately $\phi_d \pm 0.1\pi$. Although the accuracy may not be precise compared to that done by photoelectrons [45,48], it provides an alternative way to examine the IR phase and creates a new application to the HHG. Third, we use the SAP with $\tau_X = 80$ as here to achieve a better time resolution, but the method is not limited to the critical condition. Even if the SAP's width is enlarged to 300 as, the harmonic peaks and valleys are still distinguishable enough to determine the IR phase.

4. CONCLUSION

In conclusion, we theoretically study IR-driven HHG with AI attopulses, and introduce new applications based on this excitation. The conclusion is threefold. First, the control mechanism of the SAP + IR HHG is clearly elucidated using timing analysis. The ionized electrons born at a zero IR vector

potential have the longest acceleration time, and thus result in the highest cutoff energy. In contrast, ionized electrons born at peaks of the IR vector potential have the shortest acceleration time, and result in the lowest cutoff energy. However, these ionized electrons can gain an initial momentum from the IR field to move toward a high energy distribution because of the streaking effect. This increases the plateau height for ionized electrons born at peaks of the IR vector potential compared to those born at a zero IR vector potential. This effect becomes stronger as the central energy of the attopulse increases, and thus enhances the controlling capability of the plateau height. Second, in the two-color excitation the acceleration and ionization processes are exactly decoupled because of the extremely short width of the SAP. This makes it possible to resolve the IR-driven dynamics of ionized electrons from time-dependent harmonic spectra. Thus, this approach can illustrate the quantum effect on the HHG. The SAP + IR excitation provides a practical way to observe the harmonic emission for an ionized electron leaving its parent ion, which is in the semi-classically forbidden situation. Third, the realistic pulse shape of the SAP and IR field is quantitatively important in controlling HHG. A finite SAP's width shall weaken the controlling capability of the cutoff energy, and thus the SAP's width should be minimized in this HHG application. In contrast, the IR pulse shape has a positive strong effect on controlling the cutoff energy. Based on this effect, the IR carrier-envelope phase could be experimentally determined by the SAP + IR harmonic spectra with the assistance of some calibration calculations.

ACKNOWLEDGMENTS

This research is supported by National Science Council, Taiwan, under the NSC contracts 100-2112-M-009-006-MY3 and NSC 97-2811-M-009-055.

REFERENCES

1. F. Krausz and M. Ivanov, "Attosecond physics," Rev. Mod. Phys. **81**, 163–234 (2009).
2. M. Nisoli and G. Sansone, "New frontiers in attosecond science," Prog. Quantum Electron. **33**, 17–59 (2009).
3. M. Drescher, M. Hentschel, R. Kienberger, M. Uiberacker, V. Yakovlev, A. Scrinzi, T. Westerwalbesloh, U. Kleineberg, U. Heinzmann, and F. Krausz, "Time-resolved atomic inner-shell spectroscopy," Nature **419**, 803–807 (2002).
4. M. Uiberacker, T. Uphues, M. Schultze, A. J. Verhoef, V. Yakovlev, M. F. Kling, J. Rauschenberger, N. M. Kabachnik, H. Schröder, M. Lezius, K. L. Kompa, H.-G. Muller, M. J. J. Vrakking, S. Hendel, U. Kleineberg, U. Heinzmann, M. Drescher, and F. Krausz, "Attosecond real-time observation of electron tunnelling in atoms," Nature **446**, 627–632 (2007).
5. M. Wickenhauser, J. Burgdöfer, F. Krausz, and M. Drescher, "Time resolved Fano resonances," Phys. Rev. Lett. **94**, 023002 (2005).
6. Z. X. Zhao and C. D. Lin, "Theory of laser-assisted autoionization by attosecond light pulses," Phys. Rev. A **71**, 060702 (2005).
7. T. Morishita, S. Watanabe, and C. D. Lin, "Attosecond light pulses for probing two-electron dynamics of helium in the time domain," Phys. Rev. Lett. **98**, 083003 (2007).
8. E. Goulielmakis, Z.-H. Loh, A. Wirth, R. Santra, N. Rohringer, V. S. Yakovlev, S. Zherebtsov, T. Pfeifer, A. M. Azzeer, M. F. Kling, S. R. Leone, and F. Krausz, "Real-time observation of valence electron motion," Nature **466**, 739–743 (2010).
9. K. Klünder, J. M. Dahlström, M. Gisselbrecht, T. Fordell, M. Swoboda, D. Guénot, P. Johnsson, J. Caillat, J. Mauritsson, A. Maquet, R. Taïeb, and A. L. Huillier, "Probing single-photon ionization on the attosecond time scale," Phys. Rev. Lett. **106**, 143002 (2011).
10. T. Remetter, P. Johnsson, J. Mauritsson, K. Varjú, Y. Ni, F. Lépine, E. Gustafsson, M. Kling, J. Khan, R. López-Martens, K. J. Schafer, M. J. J. Vrakking, and A. L. Huillier, "Attosecond electron wave packet interferometry," Nat. Phys. **2**, 323–326 (2006).
11. P. Johnsson, R. López-Martens, S. Kazamias, J. Mauritsson, C. Valentin, T. Remetter, K. Varjú, M. B. Gaarde, Y. Mairesse, H. Wabnitz, P. Salières, P. Balcou, K. J. Schafer, and A. L. Huillier, "Attosecond electron wave packet dynamics in strong laser fields," Phys. Rev. Lett. **95**, 013001 (2005).
12. P. Johnsson, J. Mauritsson, T. Remetter, A. L'Huillier, and K. J. Schafer, "Attosecond control of ionization by wave-packet interference," Phys. Rev. Lett. **99**, 233001 (2007).
13. X. M. Tong, P. Ranitovic, C. L. Cocke, and N. Toshima, "Mechanisms of infrared-laser-assisted atomic ionization by attosecond pulses," Phys. Rev. A **81**, 021404(R) (2010).
14. L. Y. Peng, E. A. Pronin, and A. F. Starace, "Attosecond pulse carrier-envelope phase effects on ionized electron momentum and energy distributions: roles of frequency, intensity and additional IR pulse," New J. Phys. **10**, 025030 (2008).
15. F. Kelkensberg, W. Siu, J. F. Pérez-Torres, F. Morales, G. Gademann, A. Rouzée, P. Johnsson, M. Lucchini, F. Calegari, J. L. Sanz-Vicario, F. Martín, and M. J. J. Vrakking, "Attosecond control in photoionization of hydrogen molecules," Phys. Rev. Lett. **107**, 043002 (2011).
16. F. He and U. Thumm, "Dissociative ionization of H_2 in an attosecond pulse train and delayed laser pulse," Phys. Rev. A **81**, 053413 (2010).
17. C. F. de M. Faria, P. Salières, P. Villain, and M. Lewenstein, "Controlling high-order harmonic generation and above-threshold ionization with an attosecond-pulse train," Phys. Rev. A **74**, 053416 (2006).
18. K. J. Schafer, M. B. Gaarde, A. Heinrich, J. Biegert, and U. Keller, "Strong field quantum path control using attosecond pulse trains," Phys. Rev. Lett. **92**, 023003 (2004).
19. C. F. de M. Faria and P. Salières, "High-order harmonic generation with a strong laser field and an attosecond-pulse train: the Dirac-Delta comb and monochromatic limits," Laser Phys. **17**, 390–400 (2007).
20. E. J. Takahashi, T. Kanai, K. L. Ishikawa, Y. Nabekawa, and K. Midorikawa, "Dramatic enhancement of high-order harmonic generation," Phys. Rev. Lett. **99**, 053904 (2007).
21. J. Biegert, A. Heinrich, C. P. Hauri, W. Kornelis, P. Schlup, M. Anscombe, K. J. Schafer, M. B. Gaarde, and U. Keller, "Enhancement of high-order harmonic emission using attosecond pulse trains," Laser Phys. **15**, 899–902 (2005).
22. P. B. Corkum, "Plasma perspective on strong field multiphoton ionization," Phys. Rev. Lett. **71**, 1994–1997 (1993).
23. M. Lewenstein, P. Balcou, M. Yu. Ivanov, A. L'Huillier, and P. B. Corkum, "Theory of high-harmonic generation by low-frequency laser fields," Phys. Rev. A **49**, 2117–2132 (1994).
24. D. B. Milošević, "Theoretical analysis of high-order harmonic generation from a coherent superposition of states," J. Opt. Soc. Am. B **23**, 308–317 (2006).
25. K. L. Ishikawa, "Photoemission and ionization of He^+ under simultaneous irradiation of fundamental laser and high-order harmonic pulses," Phys. Rev. Lett. **91**, 043002 (2003).
26. H. C. Lee and T. F. Jiang, "Control mechanism of atomic ionization and high-order harmonic generation assisted by attosecond pulses," Appl. Phys. B **109**, 621–630 (2012).
27. E. J. Takahashi, P. Lan, Oliver D. Mücke, Y. Nabekawa, and K. Midorikawa, "Infrared two-color multicycle laser field synthesis for generating an intense attosecond pulse," Phys. Rev. Lett. **104**, 233901 (2010).
28. E. Mansten, J. M. Dahlström, P. Johnsson, M. Swoboda, A. L'Huillier, and J. Mauritsson, "Spectral shaping of attosecond pulses using two-colour laser fields," New J. Phys. **10**, 083041 (2008).
29. J. J. Carrera, X. M. Tong, and S. I. Chu, "Creation and control of a single coherent attosecond xuv pulse by few-cycle intense laser pulses," Phys. Rev. A **74**, 023404 (2006).
30. C. K. Chui, *An Introduction to Wavelets* (Academic, 1992).
31. X. M. Tong and S. I. Chu, "Probing the spectral and temporal structures of high-order harmonic generation in intense laser pulses," Phys. Rev. A **61**, 021802 (2000).

32. J. A. Pérez-Hernández and L. Plaja, "Quantum description of the high-order harmonic generation in multiphoton and tunneling regimes," Phys. Rev. A **76**, 023829 (2007).
33. H. C. Lee, S. D. Jheng, and T. F. Jiang, "Theory of infrared-dressed atomic photoionization by extremely ultraviolet attosecond pulse trains," J. Opt. Soc. Am. B **29**, 286–293 (2012).
34. X. M. Tong and C. D. Lin, "Empirical formula for static field ionization rates of atoms and molecules by lasers in the barrier-suppression regime, " J. Phys. B **38**, 2593–2600 (2005).
35. O. Smirnova, M. Spanner, and M. Ivanov, "Coulomb and polarization effects in sub-cycle dynamics of strong-field ionization," J. Phys. B **39**, S307–S321 (2006).
36. O. Smirnova, M. Spanner, and M. Y. Ivanov, "Coulomb and polarization effects in laser-assisted XUV ionization," J. Phys. B **39**, S323–S339 (2006).
37. O. Smirnova, M. Spanner, and M. Y. Ivanov, "Analytical solutions for strong field-driven atomic and molecular one- and two-electron continua and applications to strong-field problems," Phys. Rev. A **77**, 033407 (2008).
38. M. Ivanov and O. Smirnova, "How accurate is the attosecond streak camera?," Phys. Rev. Lett. **107**, 213605 (2011).
39. J. M. Dahlström, A. L'Huillier, and A. Maquet, "Introduction to attoseond delays in photoionization," J. Phys. B **45**, 183001 (2012).
40. E. Goulielmakis, M. Schultze, M. Hofstetter, V. S. Yakovlev, J. Gagnon, M. Uiberacker, A. L. Aquila, E. M. Gullikson, D. T. Attwood, R. Kienberger, F. Krausz, and U. Kleineberg, "Single-cycle nonlinear optics," Science **320**, 1614–1617 (2008).
41. D. J. Jones, S. A. Diddams, J. K. Ranka, A. Stentz, R. S. Windeler, J. L. Hall, and S. T. Cundiff, "Carrier-envelope phase control of femtosecond mode-locked lasers and direct optical frequency synthesis," Science **288**, 635–639 (2000).
42. S. T. Cundiff and J. Ye, "Colloquium: femtosecond optical frequency combs," Rev. Mod. Phys. **75**, 325–342 (2003).
43. J. L. Hall, "Nobel lecture: defining and measuring optical frequencies," Rev. Mod. Phys. **78**, 1279–1295 (2006).
44. T. W. Hänsch, "Nobel lecture: passion for precision," Rev. Mod. Phys. **78**, 1297–1309 (2006).
45. G. G. Paulus, F. Lindner, H. Walther, A. Baltuška, E. Goulielmakis, M. Lezius, and F. Krausz, "Measurement of the phase of few-cycle laser pulses," Phys. Rev. Lett. **91**, 253004 (2003).
46. P. Dietrich, F. Krausz, and P. B. Corkum, "Determining the absolute carrier phase of a few-cycle laser pulse," Opt. Lett. **25**, 16–18 (2000).
47. E. Goulielmakis, M. Uiberacker, R. Kienberger, A. Baltuska, V. Yakovlev, A. Scrinzi, T. Westerwalbesloh, U. Kleineberg, U. Heinzmann, M. Drescher, and F. Krausz, "Direct measurement of light waves," Science **305**, 1267–1269 (2004).
48. T. Wittmann, B. Horvath, W. Helml, M. G. Schätzel, X. Gu, A. L. Cavalieri, G. G. Paulus, and R. Kienberger, "Single-shot carrier–envelope phase measurement of few-cycle laser pulses," Nat. Phys. **5**, 357–362 (2009).